THE JOURNAL OF BIOLOGICAL CHEMISTRY VOL. 288, NO. 12, pp. 8619–8626, March 22, 2013

Testing the Sulfotransferase Molecular Pore Hypothesis*

Received for publication, December 26, 2012, and in revised form, January 24, 2013 Published, JBC Papers in Press, January 28, 2013, DOI 10.1074/jbc.M112.445015

Ian Cook[‡], Ting Wang[‡], Steven C. Almo[§], Jungwook Kim[§], Charles N. Falany[¶], and Thomas S. Leyh[‡1]

From the Departments of [‡]Microbiology and Immunology and [§]Biochemistry, Albert Einstein College of Medicine, Bronx, New York 10461-1926 and [¶]Department Pharmacology and Toxicology, University of Alabama School of Medicine, Birmingham, Alabama 35294-0019

Background: Human cytosolic sulfotransferases (SULTs) regulate the bioactivities of hundreds of signaling molecules.
Results: Mutants define the structural changes that determine substrate selectivity.
Conclusion: Substrates enter the active site through a molecular pore that opens and closes in response to nucleotide binding.
Significance: SULT selectivity is a fundamental determinant of sulfur biology.

Human cytosolic sulfotransferases (SULTs) regulate the activities of hundreds of signaling metabolites via transfer of the sulfuryl moiety (-SO_3) from activated sulfate (3′-phosphoadenosine 5′-phosphosulfate) to the hydroxyls and primary amines of xeno- and endobiotics. How SULTs select substrates from the scores of competing ligands present in a cytosolic milieu is an important issue in the field. Selectivity appears to be sterically controlled by a molecular pore that opens and closes in response to nucleotide binding. This point of view is fostered by structures showing nucleotide-dependent pore closure and the fact that nucleotide binding induces an isomerization that restricts access to the acceptor-binding pocket. Molecular dynamics models underscore the importance of pore isomerization in selectivity and predict that specific molecular linkages stabilize the closed pore in response to nucleotide binding. To test the pore model, these linkages were disrupted in SULT2A1 via mutagenesis, and the effects on selectivity were determined. The mutations uncoupled nucleotide binding from selectivity and produced enzymes that no longer discriminated between large and small substrates. The mutations did not affect the affinity or turnover of small substrates but resulted in a 183-fold gain in catalytic efficiently toward large substrates. Models predict that an 11-residue "flap" covering the acceptor-binding pocket can open and admit large substrates when nucleotide is bound; a mutant structure demonstrated that this is so. In summary, the model was shown to be a robust, accurate predictor of SULT structure and selectivity whose general features will likely apply to other members of the SULT family.

Human cytosolic sulfotransferases (SULTs)[2] are broadly involved in the regulation of human metabolism and disease. This 13-member enzyme family transfers the sulfuryl moiety (-SO_3) from the universal donor 3′-phosphoadenosine 5′-phosphosulfate (PAPS; or activated sulfate) to the hydroxyls and primary amines of hundreds, perhaps thousands of acceptors (metabolites, drugs, and other xenobiotics) (1–4). Sulfonation of small molecule activators of steroid (1–3), thyroid (5), and dopamine receptors (4) typically weakens their receptor binding affinities beyond the point of physiological relevance (6). Sulfatases hydrolytically remove the sulfuryl moiety to regenerate unmodified acceptors, and the balance of SULT and sulfatase activities determines the sulfation status of a given small molecule (7). Sulfation is critical to normal functioning of a variety of processes including hemostasis (8), immune system recognition (9), lymph circulation (10), pheromone signaling (11), and growth factor recognition (12). Given its many functions in metabolism, it is not surprising that sulfonation imbalances are linked to human diseases, which include cancer of the breast and endometrium (13, 14), Parkinson disease (15), cystic fibrosis (16), and hemophilia (17).

In addition to their homeostatic roles, SULTs perform critical defensive functions in which they sulfonate and thereby inactivate scores of xenobiotics that would otherwise bind receptors and compromise signaling systems (18, 19). These two functions place very different demands on SULT selectivity. The homeostatic functions center on a relatively small set of related structures, whereas the defensive functions require that the enzymes accommodate far greater structural diversity. Apropos of the metabolic demand for dual specificity, SULTs 1A1 and 2A1 have recently been shown to isomerize between forms that exhibit widely different specificities (20). A detailed molecular description of this isomerization was the focus of the current study.

SULTs contain an active site cap that "covers" both the nucleotide- and acceptor-binding pockets (20, 21). Structures indicate that nucleotide binding closes the cap, producing a small porelike structure at the entrance to the acceptor-binding pocket (20). The sterics of this pore define the geometric limits of catalytically viable acceptors, and steric sieving may be important in sorting homeostatic from xenobiotic substrates (20). Approximately 95% of the pore is in the closed configuration when nucleotide is bound (22). The remaining 5% is in an open state, and it is in this form that nucleotide-bound SULTs can bind and sulfonate large substrates (22).

* This work was supported, in whole or in part, by National Institutes of Health Grants GM54469, GM48623, and GM38953.
The atomic coordinates and structure factors (code 4IFB) have been deposited in the Protein Data Bank (http://wwpdb.org/).
[1] To whom correspondence should be addressed: Dept. of Microbiology and Immunology, Albert Einstein College of Medicine, 1300 Morris Park Ave., Bronx, NY 10461-1926. Tel.: 718-430-2857; Fax: 718-430-8711; E-mail: tom.leyh@einstein.yu.edu.
[2] The abbreviations used are: SULT, cytosolic sulfotransferase; DHEA, dehydroepiandrosterone; PAP, 3′,5′-diphosphoadenosine; PAPS, 3′-phosphoadenosine 5′-phosphosulfate; raloxifene, [6-hydroxy-2-(4-hydroxyphenyl)-benzothiophen-3-yl]-[4-[2-(1-piperidyl)ethoxy]phenyl]methanone; MT, mutant; MD, molecular dynamics.

Molecular dynamics models of SULTs 1A1 and 2A1 have been used to predict how the structure of the active site cap responds to the binding of nucleotide (22). The caps of *in silico* SULTs open and close as nucleotide adds to and departs from the enzyme, and the models predict that specific, stabilizing molecular linkages will form as the cap closes (22). Furthermore, the models suggest that the caps subdivide into nucleotide and acceptor halves that close in a weakly coupled segmental fashion in which the acceptor segment can open and close without opening the nucleotide portion (22). The predictions of the model were tested and validated in a comparison of the substrate-selective properties and x-ray structures of the wild-type and mutant enzymes.

EXPERIMENTAL PROCEDURES

Materials

The materials and sources used in this study are as follows: dithiothreitol (DTT), EDTA, L-glutathione (reduced), glucose, imidazole, isopropyl thio-β-D-galactopyranoside, Luria broth, lysozyme, β-mercaptoethanol, pepstatin A, fulvestrant, raloxifene, 17β-estradiol, dehydroepiandrosterone (DHEA), and potassium phosphate were the highest grade available from Sigma. Ampicillin, HEPES, KOH, $MgCl_2$, NaCl, KCl, and phenylmethylsulfonyl fluoride were purchased from Fisher Scientific. Glutathione and nickel-chelating resins were obtained from GE Healthcare. Competent *Escherichia coli* (BL21(DE3)) was purchased from Novagen.

Methods

Protein Purification—SULT2A1 was inserted into a pGEX-6P expression vector with an N-terminal His/GST/maltose-binding protein tag and transformed into BL21 *E. coli* (20, 23). Mutants were generated using PCR mutagenesis and confirmed by sequencing. SULT expression and purification were performed as described previously (24). Briefly, SULT expression was induced with isopropyl 1-thio-β-D-galactopyranoside (0.30 mM). The cells were pelleted, resuspended in lysis buffer, sonicated, and centrifuged. The supernatant was loaded onto a Chelating Sepharose Fast Flow column charged with Ni^{2+}. The enzyme was eluted with imidazole (10 mM) onto a glutathione-Sepharose column and eluted with glutathione (10 mM). The tag was removed with PreScission Protease and a second glutathione column. Finally, the SULTs were concentrated using an Amicon Ultra Centrifugal Filter (molecular weight cutoff, 10 kDa). Protein concentrations were determined by UV absorbance (ϵ_{280} = 35.7 mM^{-1} cm^{-1}), and the enzyme was stored at −80 °C.

DHEA and Raloxifene Sulfation—Sulfation was measured using radiolabeled ^{3}H-acceptor. For each reaction, a solution containing SULT2A1 (50 nM; wild type (WT) or mutant (MT)), ^{3}H-acceptor (DHEA or raloxifene), $MgCl_2$ (5.0 mM), and KPO_4 (25 mM, pH 7.4) was mixed rapidly with PAPS. The concentrations of DHEA, raloxifene, and PAPS were varied from 0.2 to 5.0 times their respective K_m. Reactions were quenched by mixing the solution (10:1) with KOH (0.50 M). Sulfated and non-sulfated acceptors were separated by chloroform extraction using established protocols (2, 21). Briefly, KPO_4 (25 mM, pH 8.8) was added to the quenched solution and mixed (1:5) with chloroform. The mixture was vortexed vigorously for 15 s and centrifuged. The aqueous phase was removed and again extracted with chloroform (1:5). Sulfated acceptor in the aqueous phase was quantified using a PerkinElmer Life Sciences W450624 scintillation spectrometer. Rates were obtained from the slope of a four-point progress curve. Less than 5% of the limiting reactant was converted to product at the reaction end points. Velocities were determined in duplicate at each of the 16 conditions defined by a 4 × 4 matrix of acceptor and nucleotide concentrations. The averaged data were fit using the SEQUENO program, which uses a weighted least square fitting algorithm (25).

Fluorescence Binding Titrations—Nucleotide and acceptor binding was monitored via changes in the intrinsic fluorescence of SULT2A1 using a Cary Eclipse spectrometer (λ_{ex} = 290 nm, λ_{em} = 340 nm). Ligands were added to a solution containing SULT (50 nM), $MgCl_2$ (5.0 mM), KPO_4 (25 mM), pH 7.4 at 25 ± 2 °C. The concentration for each ligand ranged from 0.2 to 20 × K_d. Dilutions at the end points were <5.0%. Nucleotide was added from an aqueous buffered stock. Acceptor was added from a stock containing 50% ethanol. Controls ensured that the ethanol did not contribute a detectable change in fluorescence or modify the acceptor affinity. To measure the binding interactions between nucleotide and acceptor, acceptors titrations were performed at a saturating concentration of PAP (150 μM; 416 × K_d). Titrations were performed in triplicate, and the data were averaged and fit by least square analysis to a single binding site per subunit model (2, 20). The binding model and equation used to fit those data are as follows.

$$E + L \leftrightarrows E\text{-}L$$

REACTION 1

$$I/I_0 = \left(\frac{\Delta I}{I_0}\right)\frac{([E] + [L] + K_d) - (([E] + [L] + K_d)^2 - 4)[E][L])^{1/2}}{2[E]} \quad \text{(Eq. 1)}$$

E and L represent total enzyme and ligand concentrations, ΔI represents the change in fluorescence at saturating ligand, and I_0 represents the fluorescence intensity at zero ligand. Data were fit for ΔI and K_d.

Presteady State Binding—The rate constants for binding of ligands to SULT2A1 were determined by monitoring the change in enzyme fluorescence. These experiments were performed using an Applied Photophysics SX20 stopped-flow spectrometer. SULT2A1 intrinsic fluorescence (λ_{ex} = 285 nm) was detected using a cutoff filter ($\lambda_{em} \geq$ 320 nm). Sequential mixing was performed with an SQ.1 mixing accessory. A solution containing SULT2A1 (0.10 μM; WT or MT), $MgCl_2$ (5.0 mM), and KPO_4 (25 mM, pH 7.4) was rapidly mixed (1:1) with a solution lacking SULT2A1 but containing raloxifene, DHEA, or PAPS at 25 ± 2 °C. The binding of PAPS to the SULT2A1-acceptor complex was measured by adding a saturating concentration of raloxifene (50 μM; 45 × K_d) or DHEA (25 μM; 21 × K_d) to both the enzyme and PAPS solutions. SULT2A1 catalyzes a slow intrinsic hydrolysis of PAPS that must be mini-

mized in experiments that require preincubation of PAPS with enzyme, such as the binding of acceptor to the E-PAPS complex (2, 20, 22). Hydrolysis was minimized by mixing (1:1) a solution containing SULT2A1 (WT or MT; 0.20 μM), $MgCl_2$ (5.0 mM), and KPO_4 (25 mM, pH 7.4) with a solution lacking SULT2A1 but containing PAPS (400 μM) at 25 ± 2 °C. PAPS was allowed to bind for 100 ms ($\sim 5 \times t_{1/2}$) before mixing (1:1) with a solution containing DHEA or raloxifene. Hydrolysis during both mixing stages was <0.5%. All reactions were pseudo first order with respect to ligand. Three independently acquired curves were averaged to generate the data set used to obtain apparent rate constants. Rates were determined by fitting the data using Applied Photophysics Pro-Data analysis software (Marquardt fitting algorithm). k_{obs} was plotted *versus* [ligand] from which rate constants were extracted using linear least square analysis.

Crystallization and Structure Determination—In an attempt to obtain a donor-acceptor SULT2A1-L233G/L234G mutant co-crystal structure, a sample containing 600 μM PAPS and 4.7 mg/ml protein was used for initial crystallization trials. Crystals grew at 20 °C from solutions of 1.6 M NaH_2PO_4, 0.4 M K_2HPO_4, and 0.10 M phosphate-citrate, pH 4.2 and were transferred to a reservoir solution supplemented with 20% glycerol prior to flash cooling in liquid nitrogen. X-ray data were collected on an Area Detector Systems Corp. Quantum 315 charge-coupled device detector at the National Synchrotron Light Source beam line X29A and processed with HKL-3000 (26). Diffraction data were collected at a wavelength, λ, of 1.075 nm and were consistent with space group $P2_12_12_1$ (a = 73.374, b = 94.683, and c = 129.468 Å) with two molecules per asymmetric unit. Molecular replacement was performed using the PAP-bound SULT2A1 structure (Protein Data Bank code 3F3Y) as a search model with MOLREP (27). Subsequent model building and refinement was performed with Coot (28) and REFMAC5 (29). The final model was refined to 2.30 Å with R_{work} = 0.173 and R_{free} = 0.213.

RESULTS AND DISCUSSION

The Cap—The SULT2A1 active site cap (Fig. 1) is a dynamic, 30-residue stretch of amino acids (residues 224–253) that opens and closes in response to nucleotide (20, 21). In the closed state, the edge of the cap organizes into a "molecular pore" that sieves from its environment only acceptors whose dimensions lie within the thresholds of the pore (20); in the open state, these thresholds increase dramatically, allowing the enzyme to operate on a far larger set of acceptors (20). The cap is predicted to transition between a stable, well defined closed structure and an essentially structureless, highly dynamic open state (22). Nucleotide binding induces cap closure; however, simulations suggest that the acceptor half of the cap can intermittently "peel" away from the base of the binding pocket, allowing access to large substrates when nucleotide is bound. This *in silico* isomerization is consistent with recent experimental work that describes a nucleotide-driven, substrate-selective isomerization (22).

In silico models provide a dynamic, atomic-molecular description of the behavior of SULT2A1 with and without bound ligand (22). To test the integrity of the model, molecular interactions predicted to be critical to isomerization and selectivity were disrupted via mutagenesis, and the effects of these disruptions on isomerization and selectivity were determined. The target interactions are labeled *1–3* in Fig. 1. Each of these linkages is broken as the cap opens and is highly conserved among human cytosolic sulfotransferases. Links 1 and 2 couple the cap to the base of the active site through hydrophobic and salt bridge interactions, respectively. Link 3, an intracap salt linkage, fosters closure by stabilizing a structural "kink" in the cap. Link 3 is conserved either as salt bridge or π-stacking interaction. Links 1 and 2 are situated in the acceptor half of the cap; link 3 is located in the nucleotide half. MD simulations predict that weakening any of these linkages will destabilize the closed cap and should uncouple cap closure from nucleotide binding (22).

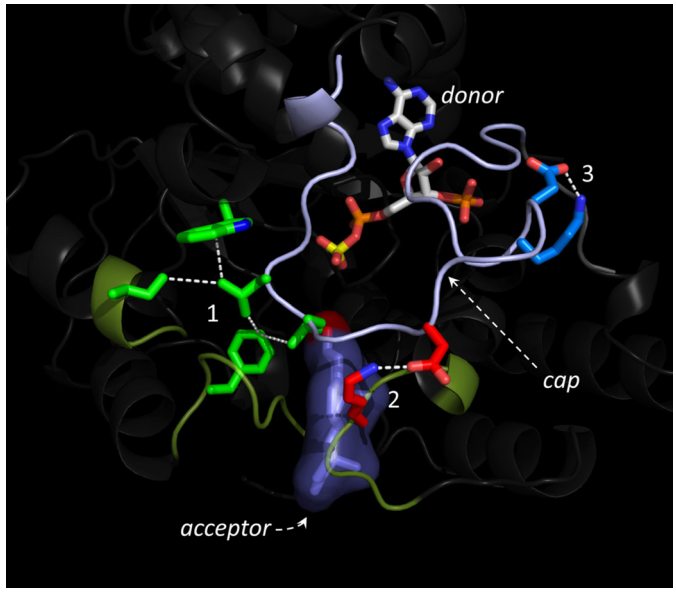

FIGURE 1. **The active site cap of SULT2A1.** The energy-minimized structure of the E-PAP complex of SULT2A1 (Protein Data Bank code 1EFH) is presented. The three molecular linkages predicted by MD models to be important in stabilizing the closed cap are color-coded and labeled as follows: *green* (*1*), *red* (*2*), and *blue* (*3*). Two residues (Val-240 and Asp-241) were disordered in the structure and were added prior to minimization. The structure and position of the cap were essentially unaltered by the minimization (root mean square deviation between the minimized and non-minimized cap is 0.117 Å). The non-minimized cap is shown in *light blue* in Fig. 5. The sulfuryl moiety of PAP and the acceptor (DHEA) were added as visual cues. DHEA was docked into the closed structure using GOLD (32).

The Mutations—The hydrophobic interactions (link 1) were disrupted by replacing isoleucine at positions 233 and 234 with glycine. This substitution replaces the hydrophobic isobutyryl moieties of isoleucine with a proton and will likely enhance loop flexibility. The salt linkages were weakened by replacing aspartate at either link 2 (Asp-237) or 3 (Asp-241) with serine. This substitution removes a single oxygen atom from the protein and should substantially weaken if not completely abolish the ionic interaction.

The Assay Strategy—Nucleotide binding controls selectivity by constricting a pore that restricts access to the acceptor-binding pocket. The enzyme maintains the ability to bind and sulfonate large substrates by isomerizing between open and closed states. With nucleotide bound, the isomerization equilibrium constant, K_{iso}, is 21 in favor of the closed form of SULT2A1 (20). Although the affinities of acceptors small enough to pass

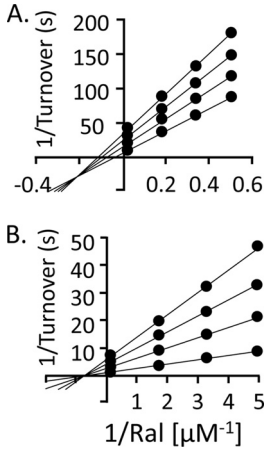

FIGURE 2. **Raloxifene sulfation by wild-type and mutant SULT2A1.** *A*, sulfation by WT SULT2A1. Initial rates were determined at the 16 conditions defined by a 4 × 4 matrix of PAPS and raloxifene (*Ral*) concentrations. Substrate concentrations were varied from 0.20 to 5.0 × K_m in equal increments in double reciprocal space. Less than 5% of the concentration-limiting substrate converted to product at the reaction end point was consumed during the reaction. The conditions were: SULT2A1 (0.20 μM), $MgCl_2$ (5.0 mM), and KPO_4 (0 mM, pH 7.4) at 25 ± 2 °C. *B*, sulfation by L233G/L234G SULT2A1. The experimental design and conditions were identical to those of *A*. Each *point* represents the average of two independent determinations. The *lines* through the points represent the best fit behavior predicted by a sequential Bi-Bi model. The kinetic constants are presented in Table 1.

through the pore are not affected by nucleotide (20, 22), large substrates cannot bind without paying an energetic penalty equal to the "work" needed to open the pore. At saturating nucleotide, the affinity constant for large substrates, K_A, is given by $K_A = K_d(1 + K_{iso})$ where K_d is the dissociation constant for binding to the open form. The model used to derive this equation assumes that large substrate affinity for the open form is independent of whether nucleotide is bound; this is the case for the substrates used in this work (22). A mutation that weakens the interface between the cap and base is expected to decrease K_{iso} and thus lessen the effect of PAPS on large substrate affinity. Hence, the accuracy of the model can be determined by measuring the effects of mutations on the linkage between PAPS binding and large substrate affinity.

Cap Mutation Abolishes Antisynergy—The nearly identical steady-state (K_m) and equilibrium binding (K_d) affinity constants for both large and small SULT2A1 substrates indicates that substrate binding is near equilibrium during turnover (20). Consequently, K_m of a large substrate for the wild-type enzyme is expected to increase to a maximum value at saturating PAPS; this has been observed previously: saturation with PAPS causes a 21-fold increase in the K_m of raloxifene, a large substrate, but has no effect on the K_m of DHEA, a small substrate (20).

MD modeling predicts that the double mutant will substantially weaken the closed cap conformation, decreasing K_{iso} and lessening the effect of PAPS on $K_{m(raloxifene)}$. To test this, initial rate parameters for the wild-type and mutant enzymes were obtained using raloxifene and DHEA. Representative data are presented in Fig. 2, *A* and *B*, and the associated constants are compiled in Table 1. For a bisubstrate enzymatic reaction, the vertical component of the point of intersection of the lines passing through the 1/*v versus* 1/[*S*] data is given by $k_{cat}(1 - K_m/K_i)$ where K_i and K_m are the affinity constants of a substrate taken at

TABLE 1
Initial rate constants for DHEA and raloxifene (RAL) sulfation by SULT2A1

Enzyme	Substrate	K_m	K_{ia}	K_{ia}/K_m	k_{cat}
		μM	μM		s^{-1}
WT	DHEA	1.3 (0.1)[a]	1.8 (0.1)	1.4 (0.2)	0.70 (0.03)
	PAPS	0.39 (0.01)	0.47 (0.06)		
	RAL	24 (0.3)	1.1 (0.05)	0.043 (0.008)	0.10 (0.005)
	PAPS	5.9 (0.6)	0.24 (0.04)		
MT	DHEA	1.4 (0.3)	1.6 (0.1)	1.2 (0.3)	0.70 (0.1)
	PAPS	0.24 (0.02)	0.39 (0.17)		
	RAL	1.3 (0.02)	1.3 (0.04)	1.0 (0.04)	1.0 (0.01)
	PAPS	0.50 (0.05)	0.50 (0.02)		

[a] S.E. is given in parentheses.

concentrations of the complementary substrate extrapolated to zero and infinity, respectively (20, 30). If substrates are noninteracting, $K_m = K_i$, and the lines intersect on the 1/[*S*] axis; if $K_m > K_i$, substrate binding is antisynergistic, and the intercept lies below the axis. With raloxifene as a substrate, the intercept falls below the axis with the wild-type enzyme and on the axis with the mutant (Fig. 2, *A* and *B*). The mutation appears to have weakened the closed conformation to the point that PAPS no longer detectably influences the affinity of the large substrate. The kinetic constants for the mutant and wild-type enzymes with DHEA as the acceptor are virtually identical; thus, the intrinsic binding potential and catalytic machinery of the active site have not been altered by the mutation. The only discernible effect of the mutation is on the steady-state affinity of the large substrate.

A 183-Fold Gain in Efficiency—The 19-fold increase in affinity for raloxifene caused by the double mutation is accompanied by a 10-fold increase in k_{cat} (Table 1). Thus, the resulting catalytic efficiency (k_{cat}/K_m) of the enzyme toward raloxifene is increased 183-fold, a considerable gain of function, by the mutation. The concomitant effects on affinity and turnover suggest that turnover may be rate-limited by cap movement. The closed active site encapsulates nucleotide and must open for nucleotide to escape. Thus, cap destabilization caused by the mutation could enhance turnover by facilitating product release. This suggestion is consistent with the following facts: nucleotide is released more quickly from the wild-type enzyme when cap closure is prevented (20), and turnover of estrogen sulfotransferase (SULT1E1) is product release rate-limited (2, 23).

Asp-to-Ser Mutations Do Not Affect Small Substrate Initial Rate Constants—As a control to determine whether the Asp-to-Ser mutations at positions 237 and 241 alter the ability of the enzyme to sulfonate small substrates, the catalytic constants of the mutants were determined using DHEA and compared with those of the wild-type enzyme. $K_{m(DHEA)}$ and k_{cat} were not significantly affected by the mutations (see Table 2).

Cap Destabilization Uncouples Donor-Acceptor Interactions—To further test the model, ligand interactions in the wild-type and mutant enzymes were quantitated in equilibrium binding studies. Binding of nucleotide or acceptor caused significant (~30%) changes in the intrinsic fluorescence of the enzyme. Raloxifene titrations of the wild-type enzyme at zero and saturating PAP concentrations are shown in Fig. 3*A*. Saturation with PAP caused an 18-fold decrease in the affinity of raloxifene, which corresponds to a −1.7 kcal/mol interaction energy.

TABLE 2
SULT2A1 (WT and MT) kinetic constants for DHEA sulfation

Enzyme	K_m	k_{cat}	k_{cat}/K_m	K_i
	μM	s^{-1}		μM
WT	1.3 (0.1)[a]	0.7 (0.03)	0.54 (0.06)	2.9 (0.2)
L233G/L234G	1.6 (0.2)	0.8 (0.02)	0.50 (0.07)	2.4 (0.1)
D237S	1.7 (0.1)	0.9 (0.10)	0.53 (0.09)	3.0 (0.3)
D241S	1.6 (0.2)	0.7 (0.05)	0.44 (0.08)	2.3 (0.2)

[a] S.E. is given in parentheses.

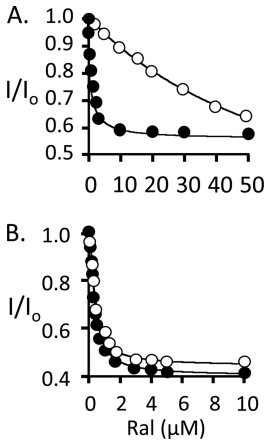

FIGURE 3. **Equilibrium binding of raloxifene to the E and E-PAP forms of SULT2A1.** *A*, binding to WT SULT2A1. Binding was monitored via intrinsic fluorescence changes of the enzyme (λ_{ex} = 290 nm, λ_{em} = 340 nm). Fluorescence changes are given relative to the intensity in the absence of raloxifene (*Ral*) (I/I_0). Solution composition was: SULT2A1 (0.50 μM), PAP (0 (●) or 125 μM (○)), $MgCl_2$ (5.0 mM), KPO_4 (50 mM, pH 7.4) at 25 ± 2 °C. *B*, binding to MT SULT2A1. The experimental design and conditions were identical to those of *A*. Each *point* represents the average of three independent determinations, and the *lines* through the points represent the behavior predicted by a best fit, single site binding model (see "Experimental Procedures"). K_d values are compiled in Table 3.

TABLE 3
DHEA and raloxifene (RAL) affinities for E and E-PAP forms of SULT2A1

	Dissociation constant			
	E		E-PAP	
Enzyme	DHEA	RAL	DHEA	RAL
		μM		
WT	1.7 (0.3)[a]	1.3 (0.2)	1.5 (0.2)	23 (2.0)
L233G/L234G	1.4 (0.3)	1.1 (0.3)	1.6 (0.2)	1.5 (0.3)
D237S	1.2 (0.4)	1.6 (0.3)	1.8 (0.4)	1.2 (0.3)
E241S	1.1 (0.3)	1.5 (0.3)	1.5 (0.2)	1.4 (0.2)

[a] S.E. is given in parentheses.

A parallel experiment with the E247S mutant revealed that this mutation, which neutralizes an ionic interaction that would otherwise stabilize the closed cap, caused the interaction between PAP and nucleotide to decrease beyond the limit of detection; however, the affinities of the nucleotide-free (open) forms of the wild-type and mutant enzymes for raloxifene are identical (Table 3). Similar studies with each mutant showed that in each case nucleotide-acceptor interactions vanished without effect on the intrinsic affinity of the open enzymes (Table 3). Thus, nucleotide-acceptor interactions can be interrupted by destabilizing the closed cap structure without altering other binding and catalytic behaviors of the enzyme.

How Open Is Open?—Measurements of the nucleotide-induced change in affinity for large substrates yield the relative stability of the closed form with and without bound nucleotide but offer no insight regarding the degree to which the cap is closed in the nucleotide-free enzyme. If the cap of the nucleotide-free, wild-type enzyme were closed in significant measure, destabilizing mutations are expected to open the cap and result in a higher affinity of raloxifene for mutant enzyme; this was not observed. The affinities of the nucleotide-free wild-type and mutant enzymes for raloxifene are identical within error; hence, the nucleotide-free enzyme favors the open state. The sensitivity of the measurements suggests that greater than 95% of the unliganded enzyme is in the open configuration.

Presteady State Binding—As PAPS concentration increases, closing the enzyme, the rate constant for large substrate binding to wild-type enzyme appears to decrease due to the decrease in the concentration of the form to which ligand binds (the open form). Escape of large substrates from the open form is independent of PAPS concentration (20). That is, the rate constant for desorption is identical whether acceptor departs from the nucleotide-free enzyme or from the small fraction of enzyme that is open when nucleotide is bound.

To determine whether mutations that destabilize the closed form alter the structural/energetic environment(s) that large substrates experience as they add to and depart from the enzyme, the on- and off-rate constants for raloxifene from the E and E-PAPS complexes of the double mutant were determined and compared with their wild-type counterparts. The binding reactions were monitored via changes in intrinsic protein fluorescence.

SULTs slowly hydrolyze PAPS. For this reason, the binding experiments involving PAPS used a two-stage mixing strategy in which enzyme is rapidly mixed with PAPS, and the solution is allowed to age for five binding reaction half-lives (~100 ms) before mixing with raloxifene. During this interval, <0.5% of PAPS was hydrolyzed. A typical binding reaction progress curve is shown in Fig. 4*A*. Reactions were pseudo first order in raloxifene, and the PAPS concentration was either zero or saturating. Apparent rate constants (k_{obs}) were obtained at a series of raloxifene concentrations by least square fitting using a single step binding model. k_{on} and k_{off} were obtained from the slopes and intercepts of the k_{obs} *versus* [raloxifene] plots shown in Fig. 4*B*. The resulting rate constants are compiled in Table 4 along with analogous constants for the wild-type enzyme (20). The rate constants for binding and dissociation of raloxifene to the E and E-PAPS forms of the double mutant are virtually identical to one another and to the constants for binding to the nucleotide-free form of the wild-type enzyme. The mutation has weakened the closed structure to the point that there are no vestiges of the closed form in either the ground- or transition-state energetics.

It is notable that the K_d values calculated from the presteady state work, which used PAPS, agree well with those from the equilibrium binding studies, which used PAP. Hence, PAP is an excellent surrogate for PAPS in binding studies, and the sulfuryl group contributes little to the interaction of the acceptor with enzyme.

The Structure of the Double Mutant—Nucleotide is encapsulated in the closed structure, and its escape requires that the cap open (20, 21). Large substrate binding to the wild-type enzyme

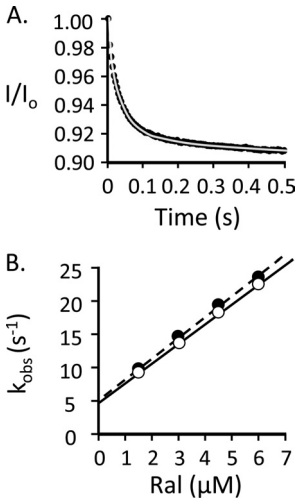

FIGURE 4. **Presteady-state binding of raloxifene to the double mutant.** *A*, binding to L233G/L234G SULT2A1. A solution containing mutant SULT2A1 (1.0 μM) was rapidly mixed (1:1) with a solution containing raloxifene (*Ral*) (12 μM) and no enzyme. Binding was observed via changes in the intrinsic fluorescence of the enzyme (λ_{ex} = 290 nm, λ_{em} ≥330 nm). Fluorescence changes are given relative to the intensity at $t = 0$ (I/I_0). *Points* represent the average of three independent determinations, and the *line* is the behavior predicted by a best fit, single exponential model. *B*, k_{obs} *versus* [raloxifene]. Reactions were pseudo first order in ligand concentration in all cases. Conditions were: PAPS (0 (●) or 150 μM (○)), $MgCl_2$ (5.0 mM), KPO_4 (25 mM), pH 7.4 at $T = 25 \pm 2$ °C. k_{obs} values were obtained from single exponential fitting of progress curves. Rate constants are compiled in Table 4.

TABLE 4
Rate constants for raloxifene (RAL) binding to SULT2A1 (WT and MT)

Enzyme	Enzyme species	k_{on}	k_{off}	K_d (k_{off}/k_{on})
		$M^{-1}\,s^{-1}$	s^{-1}	μM
MT	E○[a]	3.5 (0.1)[b] × 10^5	0.43 (0.04)	1.2 (0.1)
	PAPS-E·	3.3 (0.2) × 10^5	0.50 (0.01)	1.5 (0.2)
WT	E○	4.1 (0.1) × 10^5	0.47 (0.03)	1.1 (0.1)
	PAPS-E·	2.2 (0.3) × 10^4	0.54 (0.03)	25 (5)

[a] (·) indicates Raloxifene binding sites.
[b] S.E. is given in parentheses.

TABLE 5
Data collection and refinement statistics for the L233G/L234G SULT2A1-PAPS structure

Data collection	
Space group	$P2_12_12_1$
Cell dimension	
a, *b*, *c* (Å)	73.37, 94.68, 129.47
α, β, γ (°)	90.00, 90.00, 90.00
Resolution (Å)	50.0-2.30 (2.34-2.30)[a]
I/σ	23.5 (2.3)
Completeness (%)	100.0 (100.0)
Redundancy	5.9 (6.0)
R_{merge}	0.074 (0.744)
Refinement	
Number of reflections used	35,380
Protein non-hydrogen atoms	4,562
Ligand atoms	84
Water molecules	209
R_{work}	0.173
R_{free}	0.213
r.m.s.d.[b] from ideal geometry	
Bond Length (Å)	0.011
Bond Angles (°)	1.53

[a] Numbers in parentheses correspond to the highest resolution shell.
[b] Root mean square deviation.

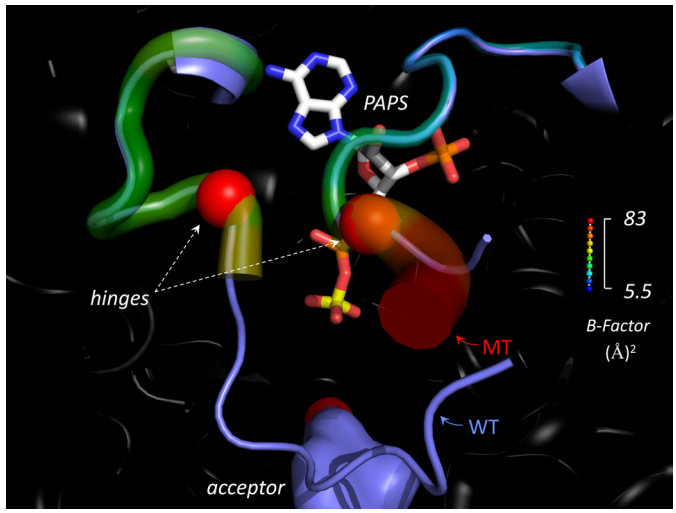

FIGURE 5. **Superposition of the active site cap of wild-type and double mutant SULT2A1.** Structures of the E-PAPS complex of wild-type (Protein Data Bank code 1EFH) and double mutant (L233G/L234G) SULT2A1 (Protein Data Bank code 4IFB) are shown. The WT cap is rendered in *blue-gray* schematic, and the MT cap is shown in *semitransparent* B-factor putty whose color and width scale with C^α B-factor. Cap orientation is similar to that in Fig. 1. Acceptor (DHEA) was docked into the Protein Data Bank 1EFH structure using GOLD (32) to provide a visual cue for the positioning of substrates. *Red spheres* identify the C^α atoms predicted by MD models to act as hinges for the opening and closure of the acceptor half of the binding pocket. The comparison shows that the acceptor segment of the MT cap indeed opens at the hinges and is completely disordered from residues 232 to 241; the WT shows disorder only at positions 240 and 241.

destabilizes the bound nucleotide exclusively through an increase in k_{off} (20). Presumably, this coupling occurs because the nucleotide portion of the cap cannot fully close while a large substrate prevents closure at the acceptor binding site. In contrast, nucleotide binding to the mutants is not affected by large substrates; coupling has disappeared. Consistent with these observations, MD simulations predict that the cap subdivides into nucleotide and acceptor halves that open and close as units (or segments). In the wild-type enzyme, nucleotide binding is predicted to be concomitant with closure of its segment, and following a brief well defined delay, the acceptor segment snaps shut (22). Neither segment reopens over a simulated 20-ns interval. In contrast, the acceptor half of the mutant cap opens and closes readily, whereas the nucleotide half remains closed (see movie in Ref. 22). Thus, the segmental motion model predicts not only the isomerization but its uncoupling from nucleotide binding.

The double mutant was crystallized in the hope of gaining insight into the structure of the mutated cap. The structure of the E-PAPS complex was obtained (see "Experimental Procedures" and Table 5), and its cap was compared with that of the wild-type complex (31) in Fig. 5. The native cap is rendered in blue-gray schematic and shows disorder (indicated by missing residues) at two residues (240 and 241). The mutant cap is shown in semitransparent B-factor putty and is disordered over 10 residues (232–241). Remarkably, only the acceptor half of the mutant cap is disordered–the nucleotide segment remains in place and is virtually indistinguishable from that of wild type. Clearly, it is possible for half of the cap to open and to do so independently of the other. The *red spheres* in Fig. 5 mark the C^α carbons predicted to act as "hinges" for the cap segments, and indeed, the mutant segment pivots at those same hinges.

Conclusions—Previous work established that PAPS binding induces an isomerization that limits access to SULT

acceptor-binding pockets, and structures with and without nucleotide provided a plausible molecular framework for that isomerization. Molecular dynamics modeling supported that that framework is the basis of the isomerization and offers a refined but untested molecular description of the response of the framework to nucleotide. The *in silico* system accurately mimics *in vitro* behavior. It predicts a substrate-selective isomerization in response to nucleotide binding and whether a particular substrate will bind to the open or closed form of the enzyme (22). It further predicts that the active site cap closes in two segments and that the segment covering the acceptor-binding site will open and close, whereas the nucleotide portion of the cap remains fixed in the closed position (22), a prediction without structural precedent until the current study.

With the goal of establishing a detailed and accurate molecular description of the nucleotide-coupled isomerization that controls SULT selectivity, the pore hypothesis was tested using mutagenesis. Single atoms and R groups predicted to be important in coupling nucleotide binding to pore formation were removed from the enzyme, and the effects of these deletions were determined. The result was a complete uncoupling of nucleotide binding and selectivity without influencing the catalytic machinery–the efficiency of the enzyme for small substrates was not affected by the mutations, whereas the efficiency toward large substrates increased 183-fold due to an enhanced affinity that arises from the inability of the mutants to form a stable pore that selects against such substrates. Remarkably, the segmental cap model that explains how the enzyme accesses large substrates when nucleotide is bound was given strong support by structural studies of the double mutant that show the acceptor segment peeled away from the base of the active site and prepared to bind large substrates, whereas the nucleotide remained bound, and its cap remained closed.

A detailed description of the molecular linkages that couple nucleotide binding, SULT2A1 isomerization, and selectivity has been outlined and tested rigorously using initial rate kinetics, equilibrium and presteady-state ligand binding studies, and x-ray crystallography. The model has proven credible at all levels tested and as such is an accurate predictor of SULT function. This validation of the *in silico* models suggests that they may be valuable in developing *in silico* screens designed to predict sulfotransferase metabolism.

REFERENCES

1. Bai, Q., Xu, L., Kakiyama, G., Runge-Morris, M. A., Hylemon, P. B., Yin, L., Pandak, W. M., and Ren, S. (2011) Sulfation of 25-hydroxycholesterol by SULT2B1b decreases cellular lipids via the LXR/SREBP-1c signaling pathway in human aortic endothelial cells. *Atherosclerosis* **214,** 350–356
2. Zhang, H., Varlamova, O., Vargas, F. M., Falany, C. N., and Leyh, T. S. (1998) Sulfuryl transfer: the catalytic mechanism of human estrogen sulfotransferase. *J. Biol. Chem.* **273,** 10888–10892
3. Parker, C. R. (1999) Dehydroepiandrosterone and dehydroepiandrosterone sulfate production in the human adrenal during development and aging. *Steroids* **64,** 640–647
4. Goldstein, D. S., Swoboda, K. J., Miles, J. M., Coppack, S. W., Aneman, A., Holmes, C., Lamensdorf, I., and Eisenhofer, G. (1999) Sources and physiological significance of plasma dopamine sulfate. *J. Clin. Endocrinol. Metab.* **84,** 2523–2531
5. Visser, T. J. (1994) Role of sulfation in thyroid hormone metabolism. *Chem. Biol. Interact.* **92,** 293–303
6. Kuiper, G. G., Carlsson, B., Grandien, K., Enmark, E., Häggblad, J., Nilsson, S., and Gustafsson, J. A. (1997) Comparison of the ligand binding specificity and transcript tissue distribution of estrogen receptors α and β. *Endocrinology* **138,** 863–870
7. Aidoo-Gyamfi, K., Cartledge, T., Shah, K., and Ahmed, S. (2009) Estrone sulfatase and its inhibitors. *Anticancer Agents Med. Chem.* **9,** 599–612
8. Anderson, J. A., Fredenburgh, J. C., Stafford, A. R., Guo, Y. S., Hirsh, J., Ghazarossian, V., and Weitz, J. I. (2001) Hypersulfated low molecular weight heparin with reduced affinity for antithrombin acts as an anticoagulant by inhibiting intrinsic tenase and prothrombinase. *J. Biol. Chem.* **276,** 9755–9761
9. Selvan, R. S., Ihrcke, N. S., and Platt, J. L. (1996) Heparan sulfate in immune responses. *Ann. N.Y. Acad. Sci.* **797,** 127–139
10. Tangemann, K., Bistrup, A., Hemmerich, S., and Rosen, S. D. (1999) Sulfation of a high endothelial venule-expressed ligand for L-selectin. Effects on tethering and rolling of lymphocytes. *J. Exp. Med.* **190,** 935–942
11. Stowers, L., and Logan, D. W. (2010) Sexual dimorphism in olfactory signaling. *Curr. Opin. Neurobiol.* **20,** 770–775
12. Mesiano, S., and Jaffe, R. B. (1997) Developmental and functional biology of the primate fetal adrenal cortex. *Endocr. Rev.* **18,** 378–403
13. Falany, J. L., Macrina, N., and Falany, C. N. (2002) Regulation of MCF-7 breast cancer cell growth by β-estradiol sulfation. *Breast Cancer Res. Treat.* **74,** 167–176
14. Falany, J. L., and Falany, C. N. (1996) Regulation of estrogen sulfotransferase in human endometrial adenocarcinoma cells by progesterone. *Endocrinology* **137,** 1395–1401
15. Steventon, G. B., Heafield, M. T., Waring, R. H., and Williams, A. C. (1989) Xenobiotic metabolism in Parkinson's disease. *Neurology* **39,** 883–887
16. Li, L., and Falany, C. N. (2007) Elevated hepatic SULT1E1 activity in mouse models of cystic fibrosis alters the regulation of estrogen responsive proteins. *J. Cyst. Fibros.* **6,** 23–30
17. Moore, K. L. (2003) The biology and enzymology of protein tyrosine *O*-sulfation. *J. Biol. Chem.* **278,** 24243–24246
18. Falany, C. N. (1997) Enzymology of human cytosolic sulfotransferases. *FASEB J.* **11,** 206–216
19. Dong, D., Ako, R., and Wu, B. (2012) Crystal structures of human sulfotransferases: insights into the mechanisms of action and substrate selectivity. *Expert Opin. Drug Metab. Toxicol.* **8,** 635–646
20. Cook, I., Wang, T., Falany, C. N., and Leyh, T. S. (2012) A nucleotide-gated molecular pore selects sulfotransferase substrates. *Biochemistry* **51,** 5674–5683
21. Cook, I. T., Leyh, T. S., Kadlubar, S. A., and Falany, C. N. (2010) Structural rearrangements of SULT2A1: effects on dehydroepiandrosterone and raloxifene sulfation. *Horm. Mol. Biol. Clin. Investig.* **1,** 7–18
22. Cook, I., Wang, T., Almo, S. C., Kim, J., Falany, C. N., and Leyh, T. S. (2013) The gate that governs sulfotransferase selectivity. *Biochemistry* **52,** 415–424
23. Sun, M., and Leyh, T. S. (2010) The human estrogen sulfotransferase: a half-site reactive enzyme. *Biochemistry* **49,** 4779–4785
24. Andreassi, J. L., 2nd, and Leyh, T. S. (2004) Molecular functions of conserved aspects of the GHMP kinase family. *Biochemistry* **43,** 14594–14601
25. Cleland, W. W. (1979) Statistical analysis of enzyme kinetic data. *Methods Enzymol.* **63,** 103–138
26. Minor, W., Cymborowski, M., Otwinowski, Z., and Chruszcz, M. (2006) HKL-3000: the integration of data reduction and structure solution—from diffraction images to an initial model in minutes. *Acta Crystallogr. D Biol. Crystallogr.* **62,** 859–866
27. Lebedev, A. A., Vagin, A. A., and Murshudov, G. N. (2008) Model preparation in MOLREP and examples of model improvement using x-ray data. *Acta Crystallogr. D Biol. Crystallogr.* **64,** 33–39
28. Emsley, P., and Cowtan, K. (2004) Coot: model-building tools for molecular graphics. *Acta Crystallogr. D Biol. Crystallogr.* **60,** 2126–2132

29. Murshudov, G. N., Vagin, A. A., and Dodson, E. J. (1997) Refinement of macromolecular structures by the maximum-likelihood method. *Acta Crystallogr. D Biol. Crystallogr.* **53,** 240–255
30. Cleland, W. W. (1970) in *The Enzymes Student Edition* (Boyer, P. D., ed) pp. 1–65, Academic Press, New York
31. Pedersen, L. C., Petrotchenko, E. V., and Negishi, M. (2000) Crystal structure of SULT2A3, human hydroxysteroid sulfotransferase. *FEBS Lett.* **475,** 61–64
32. Verdonk, M. L., Chessari, G., Cole, J. C., Hartshorn, M. J., Murray, C. W., Nissink, J. W., Taylor, R. D., and Taylor, R. (2005) Modeling water molecules in protein-ligand docking using GOLD. *J. Med. Chem.* **48,** 6504–6515